Towards treatment of liver fibrosis: Cells, targets and models

Helm, D. van der

CHAPTER 6

6

CRIPTO promotes an aggressive tumour phenotype and resistance to treatment in hepatocellular carcinoma

Danny van der Helm*, Sofia Karkampouna*, Peter C. Gray, Lanpeng Chen, Irena Klima, Joël Grosjean, Mark C. Burgmans, Arantza Farina-Sarasqueta, Ewa B. Snaar-Jagalska, Deborah M. Stroka, Luigi Terracciano, Bart van Hoek, Alexander F. Schaapherder, Susan Osanto, George N. Thalmann, Hein W. Verspaget, Minneke J. Coenraad, Marianna Kruithof-de Julio

*These authors contributed equally to this work

Journal of Pathology 2018, 245, 297-310

Abstract

Background and Aim

Hepatocellular carcinoma (HCC) is the third leading cause of cancer-related death worldwide. Despite increasing treatment options for this disease, prognosis remains poor. CRIPTO (TDGF1) protein is expressed at high levels in several human tumours and promotes oncogenic phenotype. Its expression has been correlated to poor prognosis in HCC. In this study, we aimed to elucidate the basis for the effects of CRIPTO in HCC.

Methods

We investigated CRIPTO expression levels in three cohorts of clinical cirrhotic and HCC specimens. We addressed the role of CRIPTO in hepatic tumourigenesis using Cre-loxP-controlled lentiviral vectors expressing CRIPTO in cell line-derived xenografts. Responses to standard treatments (sorafenib, doxorubicin) were assessed directly on xenograft-derived ex vivo tumour slices. CRIPTO-overexpressing patient-derived xenografts were established and used for ex vivo drug response assays. The effects of sorafenib and doxorubicin treatment in combination with a CRIPTO pathway inhibitor were tested in ex vivo cultures of xenograft models and 3D cultures.

Results

CRIPTO protein was found highly expressed in human cirrhosis and hepatocellular carcinoma specimens but not in those of healthy participants. Stable overexpression of CRIPTO in human HepG2 cells caused epithelial-to-mesenchymal transition, increased expression of cancer stem cell markers, and enhanced cell proliferation and migration. HepG2-CRIPTO cells formed tumours when injected into immune-compromised mice, whereas HepG2 cells lacking stable CRIPTO overexpression did not. High-level CRIPTO expression in xenograft models was associated with resistance to sorafenib, which could be modulated using a CRIPTO pathway inhibitor in ex vivo tumour slices.

Conclusion

Our data suggest that a subgroup of CRIPTO-expressing HCC patients may benefit from a combinatorial treatment scheme and that sorafenib resistance may be circumvented by inhibition of the CRIPTO pathway.

Introduction

Hepatocellular carcinoma (HCC) is the third leading cause of cancer-related death worldwide[1]. In the majority of cases, HCC arises on a background of cirrhosis, which may be caused by chronic exposure to damaging factors, such as chronic alcohol abuse, hepatitis B or C, and various other chronic liver diseases[2]. The invasive and metastatic potential of HCCs is an important factor causing poor prognosis of affected patients. Treatment options include resection of the tumour, liver transplantation, minimal invasive image-guided oncologic therapies such as local ablation, and transarterial therapies for the early and intermediate tumour stages[3].

Targeted systemic treatments available for advanced stage tumours or tumours progressing after locoregional therapies are the tyrosine kinase inhibitors (TKIs) sorafenib (first-line)[4] and regorafenib (second-line). Sorafenib is a tyrosine kinase (VEGFR, PDGFR, RAF) inhibitor which delays HCC progression and metastatic spread but is effective in only a minority of patients and has severe side effects[4-7]. Recently, it was shown that nivolumab, a programmed cell death protein-1 (PD-1) checkpoint inhibitor, induces durable objective responses in patients with advanced stage HCC[8]. Due to a lack of biomarkers, it remains a challenge to estimate the disease progression or responsiveness to therapies[4]. In addition to the high number of non-responders to systemic therapy, there is a high percentage of HCC patients who relapse after surgical resection or minimal invasive oncological therapies. The prognosis of HCC is often dismal, with a significant risk of tumour recurrence or insufficient response to therapies due to non-specificity of the treatments[9]. Circulating α-fetoprotein (AFP) levels have been explored as biomarkers in HCC[10]. However, detection of high levels of AFP cannot be used for diagnosis or prognosis as it does not predict tumour size, stage, or HCC progression, and is absent in 30% of HCC cases[10]. Elucidation of the basic mechanisms behind the invasive and migration properties of HCCs and the identification of markers that can predict therapeutic response and the likelihood of recurrence are needed to identify suitable personalized treatments. For example, identification of sorafenib responders versus non-responders based on biomarker expression and functional *ex vivo* assay would allow better treatment selection.

CRIPTO (teratocarcinoma-derived growth factor 1; TDGF1) is a GPI-anchored signalling protein and atypical member of the transforming growth factor (TGF) gene family[11–13]. CRIPTO has multiple binding partners and signalling functions[14,15]. It enables the signalling of a subset of TGF-β superfamily ligands, including NODAL[16], that require a co-receptor (CRIPTO or Cryptic) to bind and assemble their type I and type II signalling receptors[17]. CRIPTO also inhibits other TGF-β superfamily ligands and attenuates cytostatic TGF-β1 signalling[12]. In addition, CRIPTO can act independently of the TGF-β pathway as a secreted factor that activates c-src/MAPK/Akt signalling, a pathway that is oncogenically mutated in liver cancer[18]. Notably, each of these CRIPTO signaling functions was shown to depend on CRIPTO binding to cell surface glucose regulated protein 78 kDa (GRP78)[19]. GRP78 is strongly induced by endoplasmic reticulum (ER)

stress and, like CRIPTO, plays key roles in embryogenesis, stem cell regulation, and tumour progression[20]. In addition to its physiological roles in stem cells and embryogenesis, CRIPTO is an oncofetal protein that is silenced postnatally. Re-expression is often associated with pathological conditions such as neoplasia of the breast, prostate, ovarian, bladder, colon, skin, lung, and brain[21–29]. Recently, CRIPTO expression was correlated to poor survival and tumour recurrence in HCC patients[30]. Moreover, liver-specific deletion of GRP78 promoted maintenance of tissue homeostasis and played a protective role during ER-stress response, while elevated GRP78 levels were associated with HCC progression[31–33].

In this study, we investigated CRIPTO expression in HCC aiming to elucidate the effects of the CRIPTO pathway while also exploring its potential use as a therapeutic target. We identified a potential role for CRIPTO in therapy resistance to sorafenib, suggesting that combination treatment with an inhibitor of the CRIPTO pathway might induce a beneficial response in selected patient groups.

Materials and methods

Human specimens

Aetiopathological heterogeneity in tumours was taken into account during the selection of HCC patient material; in this study, we assessed specimens from HCV infection-driven HCC (HCC-HCV, N= 4) and alcoholic liver disease-driven HCC (HCC-ALD, N= 4). Non-cirrhotic hepatitis C (HCV) tissues (N= 5) were selected as controls. Selection of tissues was performed in agreement with the 'code of good practice'. Written informed consent was obtained from each patient included in the study. The study protocol conforms to the ethical guidelines of the 1975 Declaration of Helsinki as reflected in a priori approval by the institution's Human Research Committee (B15.006/SH/sh, biobank METC MDL/009/NV/nv). Tissue microarrays (TMAs) used were from the Pathology Department of University Hospital Basel (N= 234 tissue samples including 33 HCC–adjacent tissue matched pairs) and a commercially available TMA (BC03117; US Biomax, Rockville, MD, USA; N= 69 tissue samples including seven HCC–adjacent tissue matched pairs).

Animal models

Animal protocols were approved by the Committee for Animal Experimentation and the Veterinary authorities of the Canton of Bern, Switzerland (BE55/16). Mice received food and water *ad libitum* and were housed in individually ventilated cages. NOD.Cg-Prkdc^{scid} Il2rg^{tm1Wjl}/SzJ (NSG) mice were injected subcutaneously with 0.5 × 10E6 HepG2-CRIPTO (*n*=4) or HepG2-MOCK (*n*=3) cells in Matrigel (354234; Corning, Kaiserslautern, Germany). Tumour growth was monitored weekly. At week 12, mice were sacrificed and tumours collected for further analysis.

Patient-derived xenograft (PDX)

A tumour needle biopsy from an anonymized advancedstage HCC patient was subcutaneously implanted in NSG mice and routinely passaged *in vivo*. A zebrafish line [Tg(fli1:GFP)i114] was handled and maintained according to local animal welfare regulations to standard protocols (http: //www.ZFIN.org). Two days post-fertilization (dpf), dechorionated zebrafish embryos were anaesthetized and injected with approximately 200 HepG2-MOCK or HepG2-CRIPTO cells fluorescently labelled as described previously[34]. Two days after injection, the embryos were imaged and clumps of cells (foci) counted. Zebrafish embryos (including non-injected controls) were maintained at 33 °C, to compromise between the optimal temperature requirements for fish and mammalian cells. Data are representative of/from at least two independent and blind experiments with ≥ 30 embryos per group. Foci were counted using Leica Application Suite X software (version 1.1.0.12420; Leica Biosystems BV, Amsterdam, The Netherlands).

Ex vivo tumour tissue culture and organoid generation

Tissues from HCC PDX or HepG2-CRIPTO-derived tumours were maintained in *ex vivo* cultures. Tissue slices (150–200 µm) were cultured using Transwell plates with an attached nitrocellulose membrane (Thin-Cert #662640 inserts for 24-well plates, 0.4 µm pore size; Greiner Bio-One, Kremsmünster, Austria) that allowed contact of the tissue with the growth medium but not the plastic in a manner that prevented alteration of the tissue[35,36]. Culture plates were placed in a sealed container saturated with oxygen, 40–50%, at 37 °C. Cultures were maintained for 7 days. Organoids were derived from the bulk of PDX tumours similarly to previously developed methods[37,38]. Single cell suspensions were obtained by enzymatic homogenization of the tissue by collagenase type II (Gibco, St-Sulpice VD, Switzerland) (5 mg/ml) and Accutase (Sigma, Buchs, Switzerland), followed by red blood cell lysis. Organoids were maintained in low attachment plates (Corning, Wiesbaden, Germany) in defined media (supplementary material, Table S1). Tumour slices and organoids were incubated for 7 and 2 days, respectively, with dimethyl sulphoxide (DMSO, 0.1%), DMSO plus Control-Fc antibody (2 µg/ml), sorafenib (1 µM), doxorubicin (1 µg/ml), and GRP78 N20 blocking peptide (sc1050P, 2 µg/ml; Santa Cruz, LabForce, Muttenz, Switzerland). After treatment, tissues were processed for histology.

Cell lines and CRIPTO overexpression

The HepG2 cell line was maintained in Dulbecco's Modified Eagle medium (DMEM) supplemented with 10% fetal calf serum (FCS; Gibco) and 1% penicillin/streptomycin (P/S; Invitrogen, Paisley, UK). Lentiviral pTomo-mock[39] and pTomo-CRIPTO constructs (provided by Dr P Gray; sequence from ref 12) were used for HepG2 cell transduction. Selection of positive clones was based on red fluorescent protein (RFP)-based cell sorting (FACS). Activation of CRIPTO transcription was induced by lentivirus-CRE transduction, which switched off RFP expression and induced green fluorescent protein (GFP) expression. Further information is provided in the supplementary material, supplementary materials and methods.

Results

CRIPTO promotes a proliferative and mesenchymal phenotype in *in vitro* HCC cells

CRIPTO has been shown to play an important role in tumour development and progression in various cancer types; however, its role in hepatic pathologies, such as in HCC, remains understudied.

Firstly, we studied the functional effects of CRIPTO *in vitro*, by stable overexpression of CRIPTO in HepG2, an HCC-derived cell line with low tumourigenicity *in vivo*[40]. We used a lentiviral red-to-green pTOMO-CRIPTO construct in which CRE recombinase activity excises a floxed RFP cassette, which turns on CRIPTO expression and increases expression of GFP[39]. A pTOMO-MOCK lentivirus lacking the CRIPTO insert was used to generate a control cell line (HepG2-MOCK). HepG2-CRIPTO cells transduced with pTOMO-CRIPTO and CRE virus lacked RFP expression and had GFP expression as predicted (Figure 1A). HepG2-MOCK cells were also generated in the presence of viral-mediated CRE and maintained expression of RFP and weak GFP upon transduction, whereas non-transduced cells (HepG2) showed no fluorochrome (Figure 1A). CRIPTO overexpression in the HepG2-CRIPTO cells was confirmed at both the mRNA (Figure 1B) and the protein level (supplementary material, Supplemental Figure 1A). The mRNA levels of *NODAL* and *GRP78*, encoding CRIPTO interaction partners, were both induced in HepG2-CRIPTO cells (Figure 1C, D). GRP78 protein levels were reduced (supplementary material, Supplemental Figure 1B) and phosphorylated AKT (pAKT) levels were increased, indicating downstream pathway activation (supplementary material, Supplemental Figure 1C) in HepG2-CRIPTO cells. PCNA protein level differences were minor (supplementary material, Supplemental Figure 1D). HepG2-CRIPTO cells acquired a more mesenchymal phenotype relative to control cells (HepG2 WT and HepG2-MOCK), as indicated by the downregulation of *E-CADHERIN* (Figure 1E) and upregulation of EMT markers such as *VIMENTIN* (*VIM*), *ZEB-1*, *ZEB-2*, *TWIST1*, and *SNAIL-2* (Figure 1F–J). HepG2-CRIPTO cells exhibited higher expression of the cancer stem cell (CSC) markers *BMI1* and *CD44* than control cells (Figure 1L, M). EPCAM levels were also higher in HepG2-CRIPTO cells, although this difference did not reach statistical significance (Figure 1K). Additional stemness marker expression was assessed at the mRNA level: *GLI-1*, α*v INTEGRIN* (*ITGAV*), β3 *INTEGRIN* (*ITGB3*), *ALDH1A*1, *SOX2*, and *CD24* (supplementary material, Supplemental Figure 2A–F). HepG2 CRIPTO cells also had a higher proliferation rate (Figure 1N), enhanced migration (Figure 1O), and wound closure properties (Figure 1P) compared with control cells, in line with EMT-associated gene expression (Figure 1E–J).

CRIPTO overexpression induces pro-tumourigenic *in vivo* effects

We investigated possible effects of CRIPTO on the cancer phenotype *in vivo*. HepG2-CRIPTO and HepG2-MOCK cells were implanted subcutaneously in Matrigel plugs in immunodeficient mice. Tumour formation was observed at 5 weeks post-implantation; HepG2-MOCK cells formed

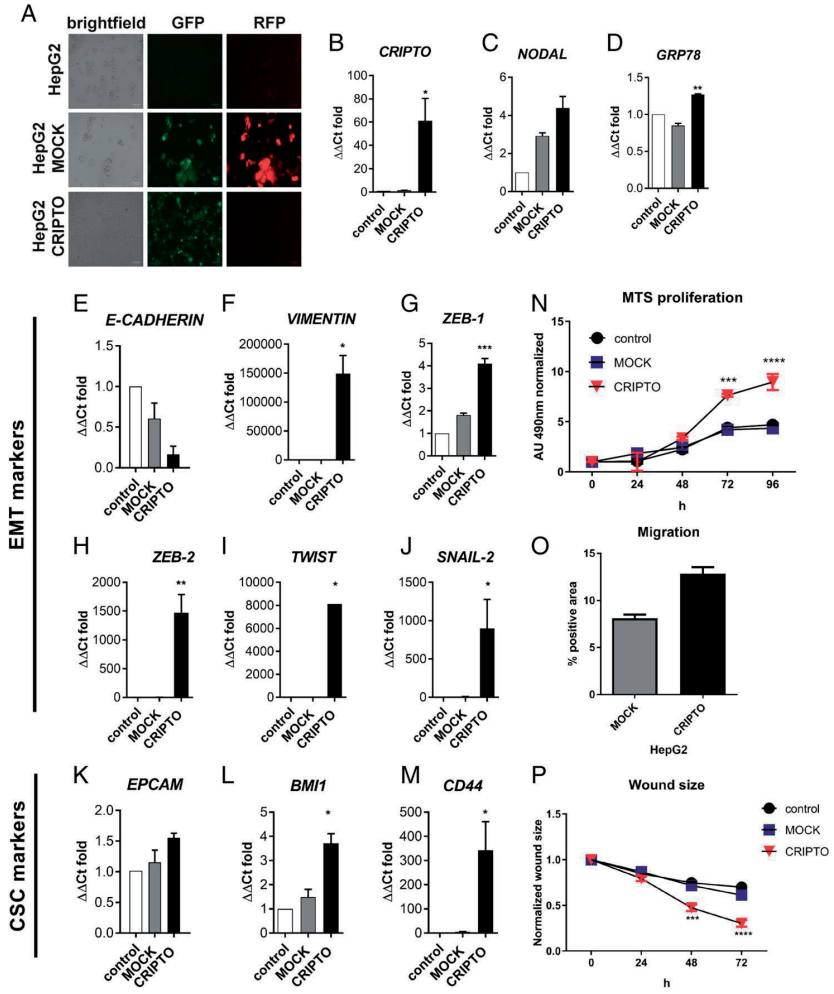

Figure 1. In vitro effects of stable overexpression of CRIPTO in HepG2 cells. (A) Cell morphology of wild-type HepG2 cells; control, stably overexpressing pTomo MOCK construct (MOCK, GFP+, RFP+); and stably overexpressing CRIPTO (CRIPTO, GFP+). Both cell lines were transduced with pTOMO and CRE lentivirus. (B–D) RT-qPCR for mRNA expression of CRIPTO-associated members of the NODAL and GRP78 pathways in (B) *CRIPTO* (*TDGF1*), (C) *NODAL*, and (D) *GRP78* mRNA expression (n=3, ±SEM). Values were normalized to *ACTB* and to control sample (ΔΔCt fold expression). (E–J) Levels of mRNA expression of epithelial-to-mesenchymal (EMT) markers in control, MOCK, and overexpressing CRIPTO HepG2 cells were assessed by RT-qPCR. (E) *E-CADHERIN* (*CDH1*); (F) *VIMENTIN* (*VIM*); (G) *ZEB-1*; (H) *ZEB-2*; (I) *TWIST1*; (J) *SNAIL-2*. Unpaired t-test; *p <0.05. (K–M) mRNA expression levels of cancer stem cell (CSC) markers. (K) *EPCAM*; (L) *BMI1*; (M) *CD44*. All values were normalized to *ACTB* and to control sample (ΔΔCt fold expression); n=3; ±SEM. Unpaired t-test; *p <0.05. (N) Metabolic activity MTS assay (24, 48, 72, 96 h) was performed in control, MOCK, and CRIPTO-overexpressing HepG2 cells. Accumulation of MTS was measured based on the absorbance at 490 nm. Values were normalized to the basal measurements at 0 h after cell seeding. The graph represents values for three independent experiments (n=3). Error bars indicate ±SEM. Two-way ANOVA; ***p <0.001; ****p <0.0001. (O) Transwell migration assay of MOCK and CRIPTO-overexpressing HepG2 cells. Quantification of percentage positive area of migrated cells (crystal violet cell dye) was performed in two independent experiments. Error bars indicate ±SEM. (P) Cell motility was assessed in wound healing (scratch) assay. Wound size was quantified in a time-dependent manner (0, 24, 48, and 72 h) in three independent experiments. Data were normalized to the 0 h time point; error bars indicate ±SEM. Unpaired t-test; *p <0.05.

Table 1. Clinical parameters of the specimens used from the LUMC cohort for mRNA analysis. The list corresponds to Figure 6A. n.a. = not applicable

qPCR cases	LUMC (N =15)
Gender, male, N (%)	11 (73.3%)
Age (range), years	72 (59–74.5)
Control (no underlying liver disease)	8 (53.3%)
Adjacent and HCC matched samples	
Fibrosis–cirrhosis (yes), N (%)	7 (46.6%)
HCC, N (%)	7 (46.6%)
T1 (N)	5
T2 (N)	1
T3 (N)	1
T4 (N)	n.a.

smaller tumours compared with the HepG2-CRIPTO-bearing mice (Figure 2A). We isolated single cells from the HepG2-CRIPTO tumour tissues and selected CRIPTO-transduced cells based on GFP expression (HepG2-CRIPTO-p1) (Figure 2B). The single cells were then injected into the duct of Cuvier of 2 dpf zebrafish embryos along with the parental HepG2-CRIPTO and HepG2-MOCK lines (Figure 2C, D) in order to determine their potential to migrate and generate tumour foci *in vivo*. HepG2-CRIPTO and HepG2-CRIPTO-p1 both showed significantly more foci at 6 dpf relative to HepG2-MOCK (Figure 2C). Histological analysis of HepG2-MOCK and HepG2-CRIPTO tumour tissues, grown as subcutaneous xenografts in mice, showed different morphological structures (Figure 2E, F); only HepG2-CRIPTO tumours resembled HCC morphology. Both tumours showed similar levels of proliferation (PCNA) (Figure 2G–I) and HNF4a liver marker expression (Figure 2J, K); however, different levels of CRIPTO were observed (Figure 2L). HepG2-MOCK xenograft tumours were distinguished by staining for the epithelial marker E-CADHERIN (Figure 2M) and absence of mesenchymal VIMENTIN expression

Figure 2. In vivo tumour formation is induced by overexpression of CRIPTO. (A) Subcutaneous tumour growth of HepG2-MOCK and HepG2-CRIPTO cells in immunocompromised mice. Tumour volumes at endpoint were calculated with calliper measurement and using the formula $V = (L \times W \times W)/2$. Average values from HepG2-MOCK (N= 3) and HepG2-CRIPTO (N= 4) are shown. Error bars indicate ±SEM. Unpaired t-test; *p <0.05. (B–D) GFP-positive HepG2-CRIPTO cells (p1) from the tumours were collected and injected in zebrafish to monitor cell migration and tumour growth (C, D) along with HepG2-MOCK and HepG2-CRIPTO cells. (E, F) Haematoxylin and eosin staining representative of the HepG2-MOCK and HepG2-CRIPTO tumours. Scale bars: 100 µm (top); 50 µm (bottom). (G–I) Immunofluorescence for PCNA (red) and cleaved caspase-3 (green) in HepG2-MOCK (G) and HepG2-CRIPTO (H) tumour sections. Scale bars: 50 µm. (I) Quantification of PCNA-positive area normalized to nuclei surface area and represented as fold change over the HepG2-MOCK samples. (J, K) Immunofluorescence for HNF4a (grey) and CRIPTO (green) in HepG2-MOCK and HepG2-CRIPTO tumour sections. Scale bars: 50 µm. (L) Quantification of CRIPTO expression (positive stained area normalized to nuclei surface area); fold change HepG2-MOCK values. (M, N) Immunofluorescence for the epithelial marker E-CADHERIN (red) in HepG2-MOCK and HepG2-CRIPTO tumour sections. Scale bars: 50 µm. (O, P). Immunofluorescence for the mesenchymal marker VIMENTIN (green) in HepG2-MOCK and HepG2-CRIPTO tumour sections. Scale bars: 50 µm.

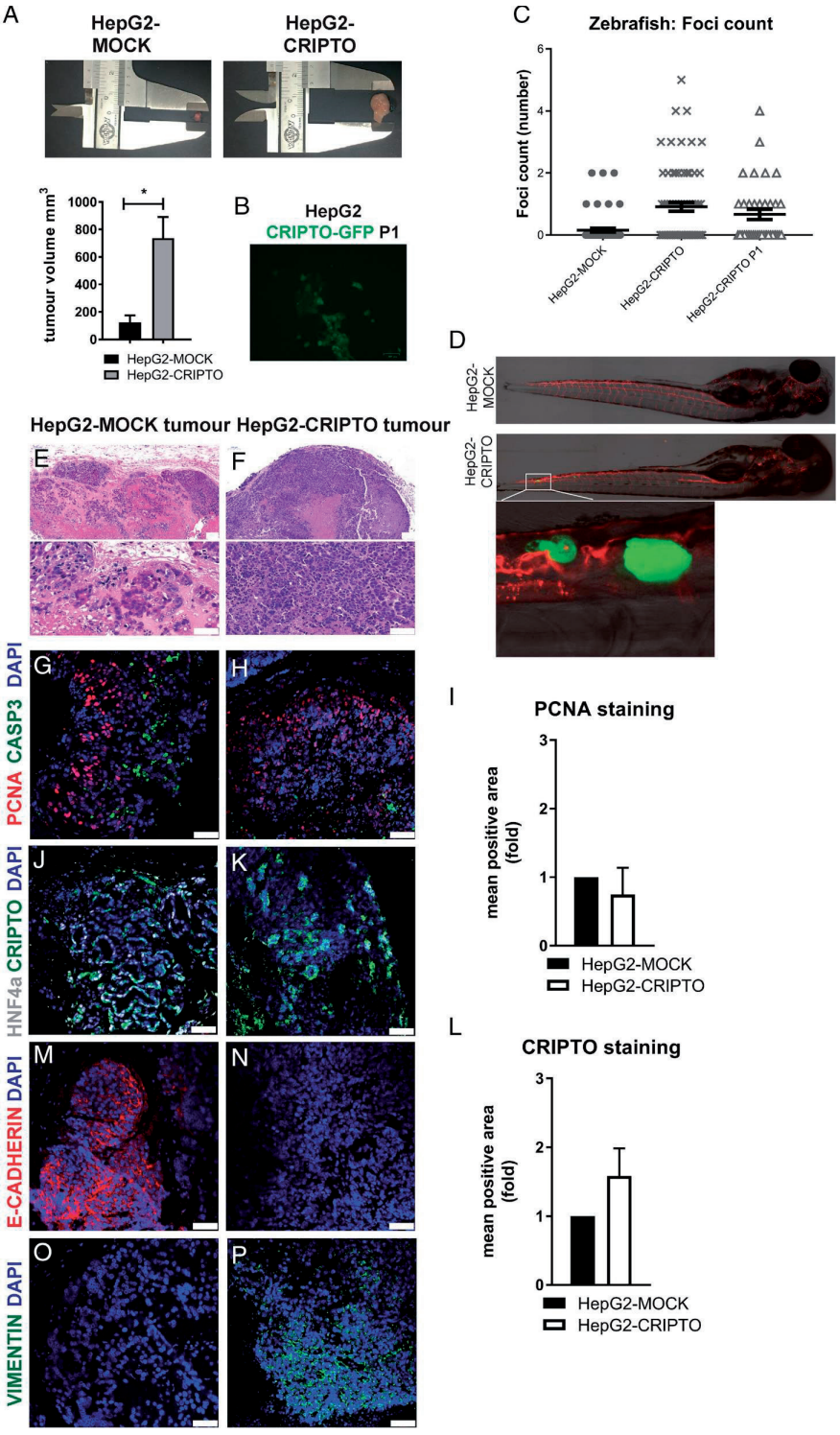
A
HepG2-MOCK
HepG2-CRIPTO
tumour volume mm3
1000
800
600
400
200
0
*
HepG2-MOCK
HepG2-CRIPTO
B
HepG2
CRIPTO-GFP P1
C
Zebrafish: Foci count
Foci count (number)
6
4
2
0
HepG2-MOCK
HepG2-CRIPTO
HepG2-CRIPTO P1
D
HepG2-MOCK
HepG2-CRIPTO
HepG2-MOCK tumour HepG2-CRIPTO tumour
E
F
G
H
PCNA CASP3 DAPI
J
K
HNF4a CRIPTO DAPI
M
N
E-CADHERIN DAPI
O
P
VIMENTIN DAPI
I
PCNA staining
mean positive area (fold)
3
2
1
0
HepG2-MOCK
HepG2-CRIPTO
L
CRIPTO staining
mean positive area (fold)
3
2
1
0
HepG2-MOCK
HepG2-CRIPTO

(Figure 2O), in contrast to the HepG2-CRIPTO tumours, which were E-CADHERIN-negative (Figure 2N) and had VIMENTIN-positive areas (Figure 2P).

HepG2-CRIPTO tumours were cultured *ex vivo* for 7 days, during which they were treated with doxorubicin or sorafenib – two compounds that are currently widely used in clinical practice for HCC treatment – in the setting of transarterial chemoembolization and oral therapy, respectively. Based on H&E staining, both treatments (Figure 3C, D) led to tissue damage compared with the untreated and vehicle (DMSO) groups (Figure 3A, B). Immunofluorescence analysis of proliferating cells (PCNA+; proliferating cell nuclear antigen-positive) indicated that doxorubicin treatment had a negative impact on tissue viability, exhibited by the absence of PCNA+ cells (Figure 3G, T). Sorafenib treatment showed areas of sustained proliferation (Figure 3H, T).

The gene expression profiles of tumours treated *ex vivo* with doxorubicin and sorafenib showed reduced CRIPTO expression (Figure 3I) in both conditions compared with control groups. However, CRIPTO expression was higher in the sorafenib condition than in the doxorubicin condition (Figure 3I). *GRP78* levels (Figure 3J) were not affected, compared with the vehicle control. *EPCAM* and *E-CADHERIN* (*CDH1*) levels were also reduced following doxorubicin and sorafenib treatment (Figure 3K, N), while *CD44* was increased significantly in both drug treatments (Figure 3M). Interestingly, only sorafenib induced expression of the stem cell marker *BMI1* (Figure 3L) and the EMT-associated genes *VIM* and *TWIST1* (Figure 3O, P). Expression of the liver cancer stem cell marker *CD24* was significantly decreased upon sorafenib treatment (supplementary material, Supplemental Figure 2G). The induction of mesenchymal (*VIM*, *TWIST1*) and stem cell markers (*CD44*, *BMI1*) by sorafenib in the HepG2-CRIPTO tumour slices may indicate an acquired aggressiveness due to CRIPTO-related activation of a resistance mechanism to sorafenib. To understand whether sorafenib resistance pre-exists in the HepG2 or is linked to CRIPTO overexpression, we assessed the proliferation rate of the HepG2 parental, control MOCK, and HepG2-CRIPTO cell lines in response to different sorafenib or doxorubicin concentrations. Proliferation, as assessed using an MTS assay, was reduced in the doxorubicinand sorafenib-treated HepG2, HepG2-MOCK, and HepG2-CRIPTO cell lines. Interestingly, HepG2 and HepG2-MOCK cells proliferated less in the presence of sorafenib (1 µM) compared with HepG2-CRIPTO (Figure 3Q–S, 96h).

CRIPTO may confer sorafenib resistance

To further investigate the role of CRIPTO in HCC, we established a patient-derived xenograft (PDX) from a needle biopsy obtained from a CRIPTO-expressing advanced cancer stage HCC prior to patient treatment with sorafenib (Figure 4A, B, original tumour and PDX1). The PDX tissue (PDX2 and PDX3 tumours) maintained both HNF4a and CRIPTO expression over time (Figure 4A, B), showing persistent proliferation (Figure 4C, D) and minimal apoptosis (Figure 4C, E) and HCC morphology (Figure 4F, G).

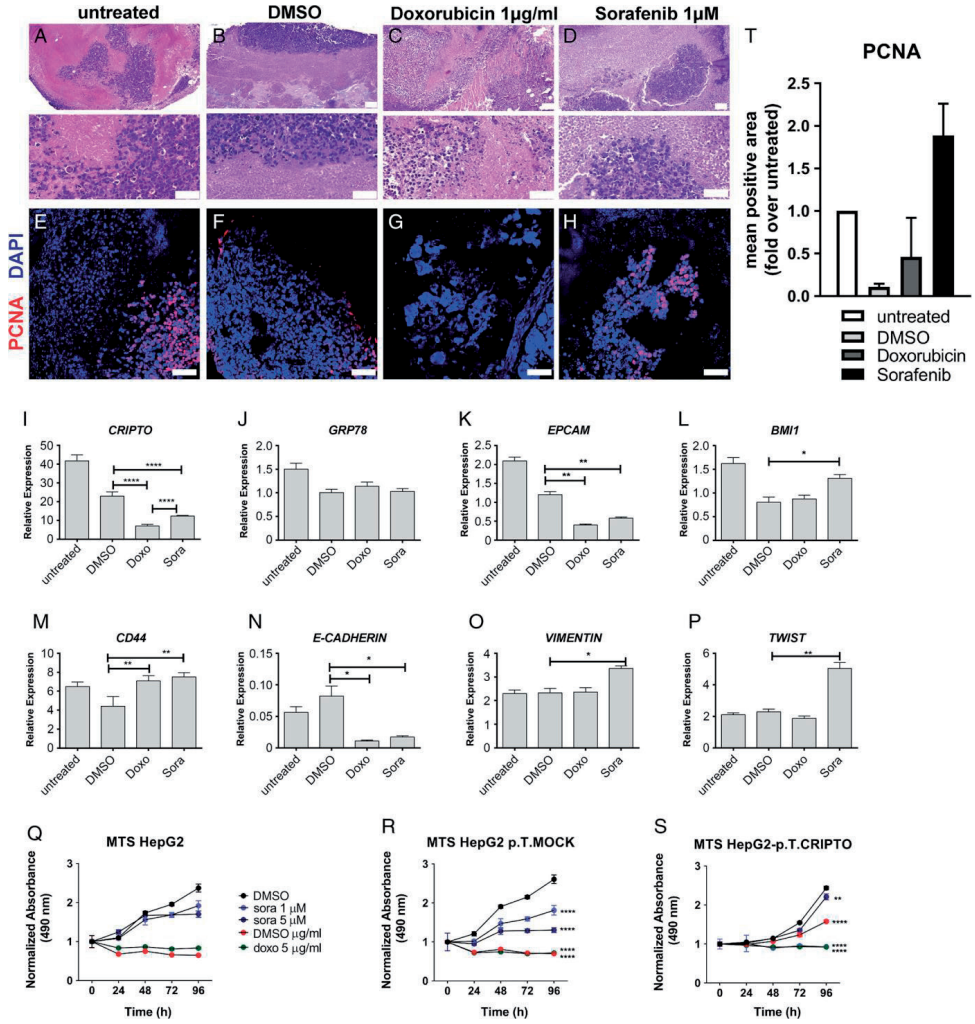

Figure 3. Ex vivo drug response to doxorubicin and sorafenib treatments indicates differential proliferation. EMT and CSC marker expression in CRIPTOhigh tumour slices *ex vivo*. (A–D) *Ex vivo* culture of HepG2-CRIPTO tumour slices; H&E staining of untreated part (A), DMSO vehicle (B), doxorubicin (1 µg/ml) (C), and sorafenib (1 µM) (D) treated. Scale bars: 100 µm (top); 50 µm (bottom). (E–H) Immunofluorescence of PCNA (red) staining on *ex vivo* cultured tissue parts; untreated part (E), DMSO vehicle (F), doxorubicin (G), and sorafenib (H) treated. DAPI marks the nuclei (blue). Scale bars: 50 µm. (I–P) Levels of mRNA for (I) *CRIPTO*, (J) *GRP78*, (K) *EPCAM*, (L) *BMI1*, (M) *CD44*, (N) *E-CADHERIN*, (O) *VIMENTIN*, and (P) *TWIST1* in HepG2-CRIPTO tumours (untreated) exposed to vehicle (DMSO), doxorubicin (1 µg/ml) (C), and sorafenib (1 µM). Unpaired *t*-test; **p* <0.05; ***p* <0.01. (Q–S) Metabolic activity MTS assay (24, 48, 72, 96 h) was performed in control (Q), MOCK- (R) and CRIPTO-overexpressing HepG2 cells (S). Cells were exposed to sorafenib (1 or 5 µM) and doxorubicin (1 or 5 µg/ml). Values are normalized to the basal measurements at 0 h after cell seeding. Graph represents values for three independent experiments (*n*=3). Error bars indicate ±SEM. Two-way ANOVA; ****p* <0.001; *****p* <0.0001. (T) Quantification of immunofluorescence staining. Mean percentage of PCNA-positive area, normalized to the nuclei (DAPI-positive area). Error bars indicate ±SD.

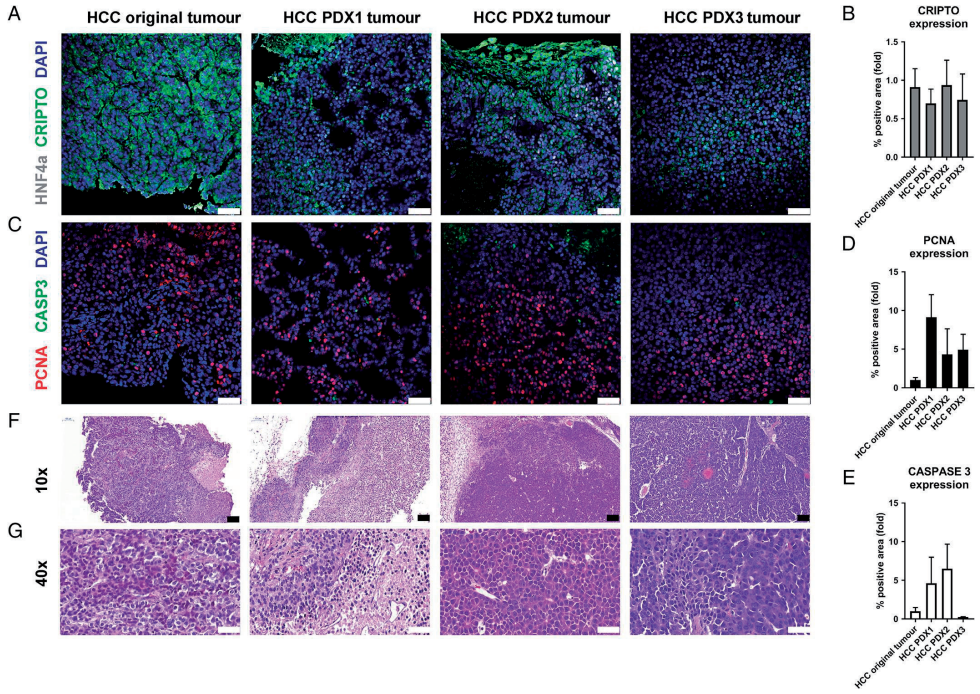

Figure 4. Establishment of CRIPTO-positive patient-derived xenograft model. (A) Immunofluorescence staining for HNF4a (grey) and CRIPTO (green) expression in an HCC tumour sample (left), HCC PDX first passage (PDX1), second passage (PDX2, centre), and third passage (PDX3, right). (B) Quantification of CRIPTO immunofluorescence staining in the PDX tumours represented as fold change the original tumour tissue expression values. Error bars indicate ±SEM. (C) Immunofluorescence staining for PCNA (red) and cleaved CASP3 (green) expression in an HCC tumour sample (left), HCC PDX first passage (PDX1), second passage (PDX2, centre), and third passage (PDX3, right). (D) Quantification of PCNA and (E) cleaved CASPASE 3 (CASP3) immunofluorescence staining in the PDX tumours represented as fold change over the original tumour tissue expression values. Error bars indicate ±SEM. (F, G) H&E staining at 10× (F) and at 40× objective (G) magnification; HCC tumour sample (left), HCC PDX first passage (PDX1), HCC PDX second passage (PDX2, centre) and third passage (PDX3, right). Scale bars 50: panels A, C and G. Scale bars 100: panel F.

To address whether CRIPTO inhibition increases tumour responsiveness to sorafenib, we employed an *ex vivo* tissue slice culture system. Tumour slices and organoids derived from the PDX (from three different passages) were treated with sorafenib; N20 (GRP78 blocking peptide), which blocks CRIPTO/GRP78 binding and CRIPTO signalling; or both in combination. Treatment with N20 blocking peptide inhibited AKT signalling activity, as shown by increased FOXO-luc activity (supplementary material, Supplemental Figure 1E).

H&E staining showed necrotic regions in all treatments in various degrees (Figure 5C–F) compared with the original and untreated condition, respectively (Figure 5A, B). Proliferation (PCNA levels) was affected in both single and combination treatments (Figure 5G–M). However, treatment with sorafenib and N20 in combination reduced cell proliferation (Figure 5L, M)

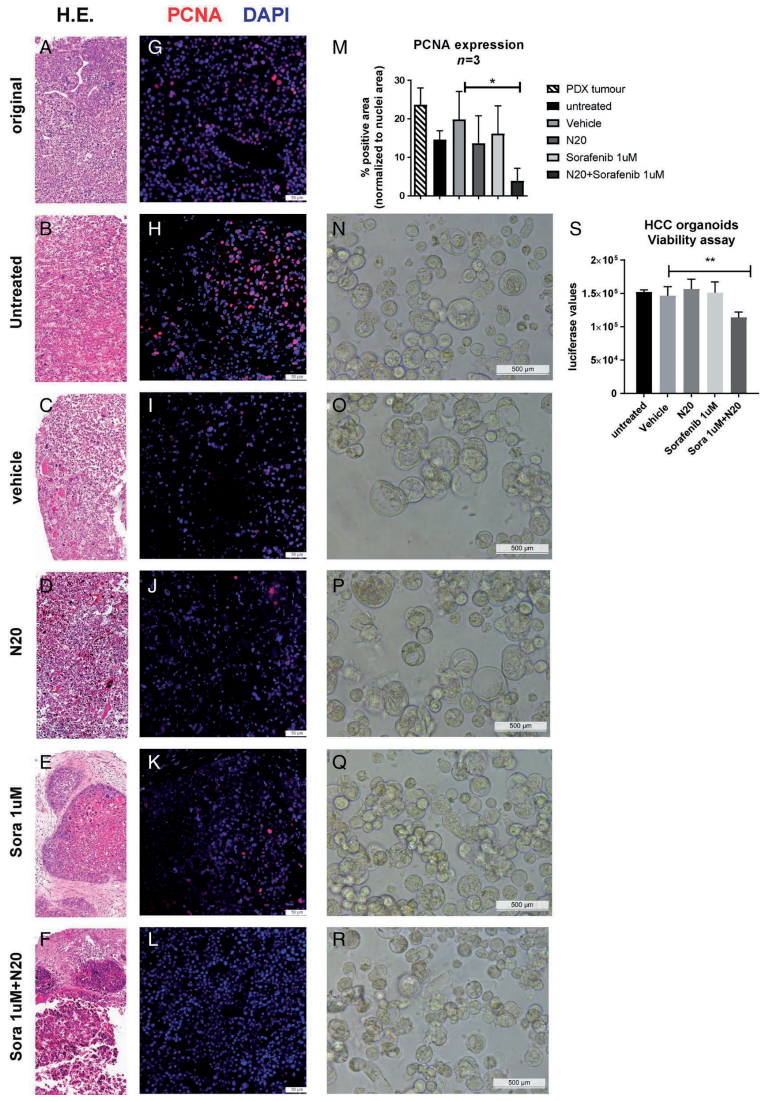

Figure 5. Sorafenib resistance may be circumvented by CRIPTO pathway inhibitor in an ex vivo culture model of HCC PDX. (A–F) *Ex vivo* tissue culture of HCC tumour tissue slices from PDX4 of the established PDX. Drug treatments were performed during the 7 days of *ex vivo* cultures. (A) Original tissue (non-cultured); (B) untreated; (C) vehicle (DMSO 0.1%) plus Control-Fc (2 µg/ml); (D) N20 blocking peptide (2 µg/ml); (E) sorafenib (1 µM); (F) sorafenib (1 µM) plus N20 (2 µg/ml). (G–L) Immunofluorescence staining for PCNA (red) and cleaved caspase-3 (green) expression. DAPI: nuclear dye. (G) Original tissue (non-cultured); (H) untreated, (I) vehicle (DMSO 0.1%) plus Control-Fc (2 µg/ml); (J) N20 blocking peptide (2 µg/ml); (K) sorafenib (1 µM); (L) sorafenib (1 µM) plus N20 (2 µg/ml). (M) Quantification of PCNA immunofluorescence staining. Mean percentage of PCNA-positive area, normalized to the nuclei (DAPI-positive area). Error bars indicate ±SEM; *n*=3 independent experiments. Paired *t*-test; **p* <0.05. (N–R) Bright-field images showing the morphology of organoids derived from the HCC PDX after 48 h of culture (N, untreated), and after treatments with (O) DMSO plus Control-Fc, (P) N20 (2 µg/ml), (Q) sorafenib (1 µM) or (R) sorafenib (1 µM) plus N20 (2 µg/ml). (S) CellTiter Glo viability luciferase-based assay measuring ATP content in organoids derived from HCC PDX tumour. Organoids were treated with DMSO plus Control-Fc, N20 (2 µg/ml), sorafenib (1 µM) or sorafenib (1 µM) plus N20 (2 µg/ml) for 48 h. Error bars indicate ±SD. Ordinary one-way ANOVA; ***p* <0.01.

to a greater extent than treatment with either of the single compounds alone. In organoid cultures derived from the PDX tumour tissue, viability, measured by CellTiterGlo assay, was also significantly reduced in the combination treatment (Figure 5N–S), indicating a higher susceptibility of sorafenib-resistant cells when CRIPTO-GRP78 signalling was blocked.

CRIPTO expression in human HCC

Expression of CRIPTO is present in embryonic tissues and becomes silenced in postnatal tissues. Reactivation of CRIPTO in adult tissues has been associated with various cancer types and thus far, only one study has investigated the role of CRIPTO in hepatic malignancy. Considering the low expression of CRIPTO at mRNA level and the absence of protein levels in human liver tissues (both obtained from http://www.proteinatlas.org), the role of CRIPTO in homeostatic and pathological liver conditions merits further investigation.

We determined the transcript levels of *CRIPTO* (*TDGF1*) in normal human liver, tumour, and tumour-adjacent tissues by RT-qPCR. Expression was low to undetectable in normal samples (*N*= 8) compared with both tumour (*N*= 7, Table 1) and tumour-adjacent (*N*= 7, cirrhotic, Table 1) tissues, which showed similar levels, indicating that increased *CRIPTO* expression is possibly associated with pre-existing chronic liver disease.

To better understand the expression pattern of CRIPTO in disease states, we determined the protein expression in a tissue microarray (TMA Basel university cohort, 234 tissue samples) by immunohistochemistry and found that HCC tissue (*N*= 128) had significantly (*p*=0.0389) less CRIPTO expression than non-HCC tissue (*N*= 106) (Figure 6B and Table 2). The non-HCC cases reflect unpaired, tumour-adjacent tissues from fibrosis, cirrhosis, and low-grade and

Figure 6. Expression of CRIPTO and its signalling partner GRP78 in human HCC liver tissues. (A) *CRIPTO* mRNA levels in tissue from healthy liver tissues (*N*= 8), tumour (*N*= 7), and tumour-adjacent tissue (*N*= 7) matched cases; values are normalized to the average of the control samples (ΔΔCt fold). (B) CRIPTO staining scoring in tissue microarray (TMA#1) samples; non-HCC (*N*= 106) versus HCC cases (*N*= 128). (C) CRIPTO protein expression in the cohort of 19 matched (tumour versus tumour-adjacent tissue) cases of TMA#1. (D–F) Representative immunofluorescence images of CRIPTO and GRP78 staining in human liver sections from HCV-derived HCC tissue (HCV infection-driven) and adjacent non-tumour control tissue from the same patient. Nuclei are stained with TO-PRO-3 (blue). Scale bars: 75 µm. Quantification of protein expression of CRIPTO (E) and GRP78 (F), determined by immunofluorescence in HCC HCV tumour (Tumour) or adjacent non-tumour tissue (Control) from the same patient (*N*= 4). Liver tissue from patients with HCV infection but absence of fibrosis (non-cirrhotic HCV, *N*= 4) was used for comparison. The percentage of positive pixel area was the average from two to four focal areas per section. Each bar represents values from each patient. Error bars indicate ±SD. (G–I) Representative immunofluorescence images of CRIPTO and GRP78 protein expression in human liver sections from alcoholic liver disease (ALD)-derived HCC tissue and adjacent non-tumour control tissue from the same patient. Nuclei are stained with TO-PRO-3 (blue). Scale bars: 75 µm. Quantification of (H) CRIPTO and (I) GRP78 protein expression as assessed by immunofluorescence in tumour HCC ALD (Tumour) and adjacent non-tumour tissue (Control) from the same patient (*N*= 4). The percentage of positive area (pixels) was the average from two to four focal areas per section. Each bar represents values from each patient. Error bars indicate ±SD. (J–L) Transcript levels for *CRIPTO* in liver tissues from normal, cirrhosis, HCC, and liver dysplasia conditions. Data were obtained from three distinct publicly available datasets (GSE14323[42], GSE14520[43], and GSE6764[41]), accessed through the Oncomine database (https://www.oncomine.org). Statistical analysis and *P* values were obtained from the Oncomine plots.

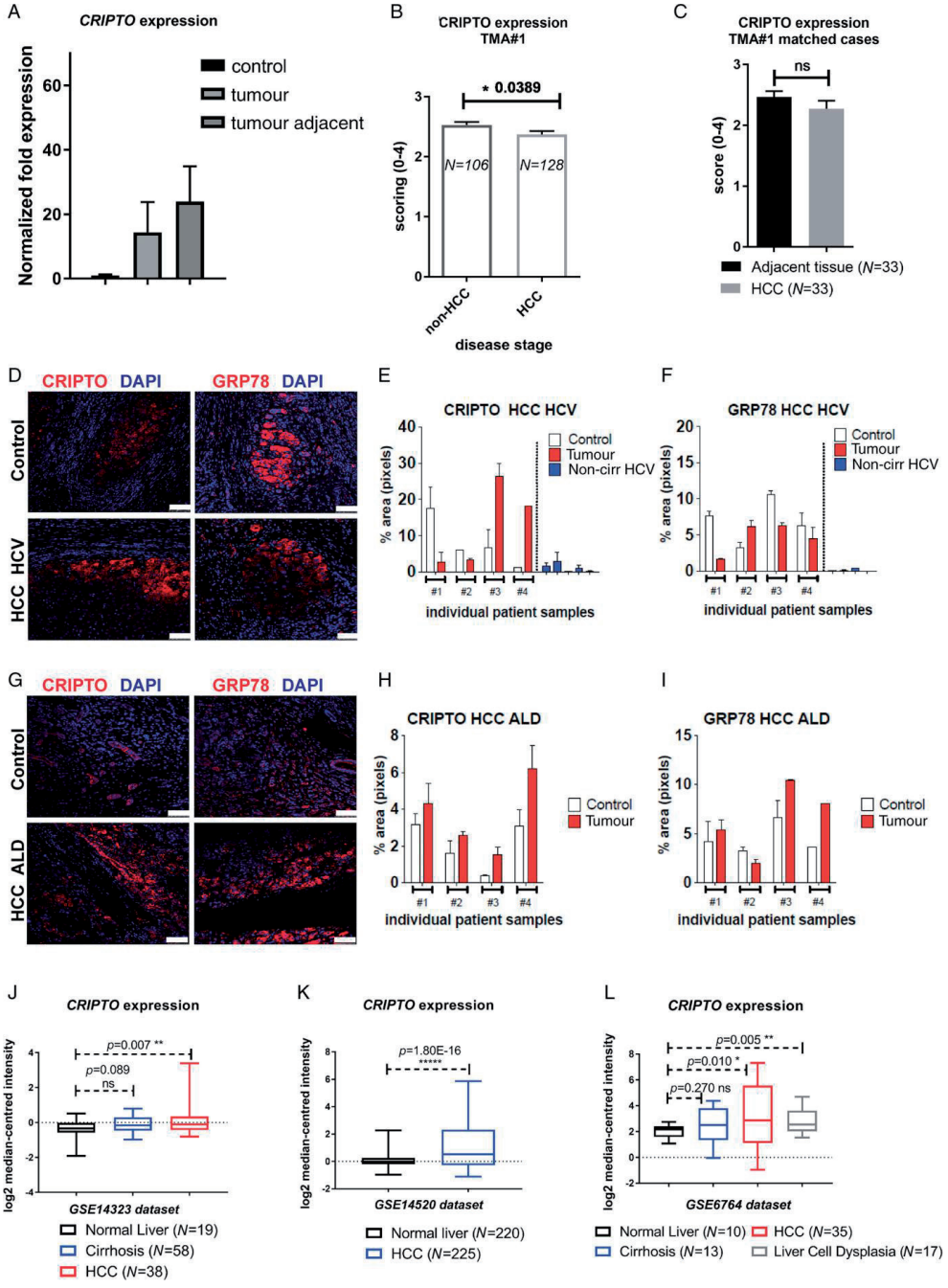
A
CRIPTO expression
Normalized fold expression
control
tumour
tumour adjacent
B
CRIPTO expression
TMA#1
* 0.0389
scoring (0-4)
N=106
N=128
non-HCC
HCC
disease stage
C
CRIPTO expression
TMA#1 matched cases
ns
score (0-4)
Adjacent tissue (N=33)
HCC (N=33)
D
CRIPTO DAPI
GRP78 DAPI
Control
HCC HCV
E
CRIPTO HCC HCV
% area (pixels)
Control
Tumour
Non-cirr HCV
individual patient samples
F
GRP78 HCC HCV
% area (pixels)
Control
Tumour
Non-cirr HCV
individual patient samples
G
CRIPTO DAPI
GRP78 DAPI
Control
HCC ALD
H
CRIPTO HCC ALD
% area (pixels)
Control
Tumour
individual patient samples
I
GRP78 HCC ALD
% area (pixels)
Control
Tumour
individual patient samples
J
CRIPTO expression
p=0.007 **
p=0.089
ns
log2 median-centred intensity
GSE14323 dataset
Normal Liver (N=19)
Cirrhosis (N=58)
HCC (N=38)
K
CRIPTO expression
p=1.80E-16
*****
log2 median-centred intensity
GSE14520 dataset
Normal liver (N=220)
HCC (N=225)
L
CRIPTO expression
p=0.005 **
p=0.010 *
p=0.270 ns
log2 median-centred intensity
GSE6764 dataset
Normal Liver (N=10)
Cirrhosis (N=13)
HCC (N=35)
Liver Cell Dysplasia (N=17)

high-grade dysplastic nodule cases (supplementary material, Supplemental Figure 3A), thus not healthy liver tissues. Within this TMA, we also analysed paired, matched cases of tumour and adjacent non-tumour tissue (*N*= 33) corresponding to the same patients and found that the CRIPTO levels were similar in both cases (Figure 6C and Table 3). A second TMA (US Biomax) was used for the validation of these results and we confirmed CRIPTO expression in both tumour-adjacent cirrhotic tissues and tumour (HCC) tissue, as in the first TMA (supplementary material, Supplemental Figure 3B, and Tables 2 and 3).

Table 2. Baseline characteristics of patients (staining samples). Patient samples correspond to Figure 6B and supplementary material, Supplemental Figure 3A (TMA Basel); Figure 6D–I (LUMC); and supplementary material, Supplemental Figure 3B (TMA US Biomax). Median (IQR). n.a. = not applicable. Only the cases with known clinical background are included in this table

Staining cases	**LUMC (N =13)**	**TMA Basel (N =163)**	**TMA US Biomax (N =62)**
Cohort with clinical background, N (%)	13 (100%)	76 (46.6%)	62 (100%)
Gender, male, N (%)	13 (100%)	58 (35.6%)	52 (83.9%)
Age (range), years	54 (47–63)	76 (67–80)	53 (45–59)
Fibrosis–cirrhosis Yes/undefined, N (%)	8 (61.5%)/n.a.	38 (23.3%)/9 (5.5%)	62 (100%)/n.a.
Patients with HCC, N (%)	8 (61.5%)	46 (28.2%)	48 (77.4%)
T1	1	15	1
T2	5	12	18
T3	2	18	25
T4	n.a.	1	4
Unknown clinical background	n.a.	87 (53.4%)	n.a.
Patients with HCC, N (%)	n.a.	82 (50.3%)	n.a.
Fibrosis–cirrhosis Yes/undefined, N (%)	n.a.	49 (30.1%)/10 (6.1%)	n.a.

Table 3. Baseline characteristics. Patient samples correspond to the matched tumour versus tumour-adjacent tissues of Figure 1A–F (LUMC); Figure 1H (TMA Basel); and supplementary material, Supplemental Figure 3 (TMA US Biomax). Median (IQR). n.a. = not applicable

Matched cases	**LUMC (N =8)**	**TMA Basel (N =33)**	**TMA US Biomax (N =7)**
Gender (male), N (%)	8 (100%)	26 (78.8%)	6 (85.7%)
Age (range), years	56.5 (51–63)	77 (68–80.5)	52 (48–54)
Fibrosis–cirrhosis Yes/ undefined, N (%)	8 (100%)	27 (81.8%)/6(18.1%)	7 (100%)
Patients with HCC, N (%)			
T1	1 (12.5%)	11 (33.3%)	n.a.
T2	5 (62.5%)	7 (21.2%)	2 (28.6%)
T3	2 (25%)	15 (45.5%)	4 (57.1%)
T4	n.a.	n.a.	1 (14.3%)

Next, we evaluated CRIPTO and GRP78 expression by immunofluorescent staining in tumours of resected human livers from HCC and adjacent cirrhotic (non-tumour) tissues (*N*= 8) and in non-cirrhotic tissues (*N*= 5, HCV infection). Clinical and tumour characteristics are shown in Table 2 (all cases) and Table 3 (matched cases). CRIPTO expression was detected at higher levels in the tumour than in adjacent cirrhotic non-tumour tissue in two out of four patients with HCV-related disease (Figure 6D, E) and in two out of four ALD-related HCC patients (*N*= 4) (Figure 6G, H). In non-cirrhotic HCV samples, we observed that expression levels of CRIPTO were lower than those of the tumour-adjacent groups (Figure 6E).

The CRIPTO binding and signalling partner GRP78 was expressed in a similar pattern with CRIPTO in hepatocytes. Quantification indicated that higher GRP78 expression in tumour tissue, as compared with adjacent non-tumorous tissue, was detected in one HCV-related (Figure 6D, F) and two ALD-related HCC patients (Figure 6G, I). In matched cases in all three TMA datasets that we have analysed here, we detected CRIPTO expression in HCC specimens both in the tumour and in the tumour-adjacent tissue – however, at different levels – and identified three subgroups of CRIPTO-expressing HCCs (Table 4).

Given the low expression of *CRIPTO* in non-cirrhotic samples (Figure 6A, E) and the high expression already in tumour-adjacent cirrhotic tissue, we accessed the transcript levels of *CRIPTO* in three microarray datasets[41–43] (publicly available data from the Oncomine database, https://www.oncomine.org). Comparison among normal liver, cirrhosis, HCC, and liver cell dysplasia indicated that HCC cases had statistically significantly higher *CRIPTO* mRNA levels versus normal liver tissues in all datasets (Figure 6J–L; $p \leq 0.01$). Cirrhotic cases showed non-significant changes (Figure 6J, L), while liver cell dysplasia showed significantly higher levels versus normal liver expression levels (Figure 6L).

The data above highlight that in individual HCCcases, evaluation of the tumour-adjacent tissue is informative but cannot be considered as control. CRIPTO expression is upregulated in many cases of pathological conditions (cirrhosis, dysplasia); thus, absolute expression levels of CRIPTO in liver tissues should be compared with reference levels from healthy tissues, and not cirrhotic, tumour-adjacent counterparts.

Table 4. Comparison of CRIPTO expression in the different cohorts of tumour versus tumour-adjacent tissue (matched cases)

Matched tissue samples	LUMC (N =8)	TMA Basel (N =33)	TMA US Biomax (N =7)
Cripto tumour < Cripto adjacent tissue, N (%)	2 (25%)	16 (48.5%)	5 (71.4%)
Cripto tumour=Cripto adjacent tissue, N (%)	0 (0%)	8 (24.2%)	1 (14.3%)
Cripto tumour > Cripto adjacent tissue, N (%)	6 (75%)	9 (27.3%)	1 (14.3%)

Discussion

CRIPTO is a cell surface protein that regulates signaling of TGF-β superfamily ligands and also has EGF-like activity. It is a small glycosylphosphatidylinositol (GPI)-anchored cell surface/ secreted oncoprotein that plays important roles in regulating stem cell differentiation, embryogenesis, tissue growth, and remodeling[14]. The tumour-promoting role of CRIPTO has been documented in multiple malignancies, including those characterized by osteotropism in their metastatic stage, such as breast and prostate cancer[25,44,45]. Recently, higher CRIPTO expression was detected in a cohort of HCC patients (49.8%, *N*= 205), and which correlated with poor prognosis[30].

We showed that CRIPTO expression in tumours was mainly detected in areas lining the stromal compartment. This is not surprising given its role in promoting EMT, which we and other groups have shown for other cancer types[46]. The CRIPTO-positive tumour cells adjacent to the stroma may enter the circulation and be responsible for metastatic spread. However, further studies are necessary to corroborate this hypothesis.

Interestingly, in the TMAs (Basel and US Biomax) that we analysed, CRIPTO protein expression was higher in the non-tumour tissue than in tumour tissue. The same trend was observed in a smaller cohort of adjacent and tumour tissue in matched cases of the TMAs, although the number of vailable matched pairs in the present study may be too small to draw firm conclusions.

Given the fact that the non-tumour tissues have a cirrhotic background and CRIPTO is not expressed during homeostasis, it could be speculated that CRIPTO correlates to disease progression[30,40]. Moreover, it should be noted that tissue sections (cores) available in the TMAs have a small size, without information of the exact location of where it was derived from within the tumour tissue. The LUMC cohort of matched cases contained large tissue areas derived from a histopathologically confirmed area (tumour, tumour-adjacent), as evaluated by a certified pathologist. It needs to be emphasized that HCCs are heterogeneous tumours and therefore the results of this study should be validated in larger numbers of matched larger tissue sections. Using a transcriptomic approach, we showed that *CRIPTO* mRNA expression is progressively elevated in pathological hepatic conditions such as HCC and liver cell dysplasia compared with normal state, as assessed in three distinct datasets (Oncomine).

In line with the human data, stable overexpression of CRIPTO in HepG2 cells led to a more aggressive tumour phenotype *in vitro*, *ex vivo* and *in vivo* characterized by EMT, mesenchymal phenotype, as well as stem cell characteristics as determined by histology and transcript level alterations. Our data support the notion that CRIPTO plays a role in cirrhosis as well as

tumour initiation and aggressiveness by increasing cellular plasticity and stem cell properties similar to what we have also shown recently for prostate cancer[34].

Elevated CRIPTO levels in both HCC and the cirrhotic, potentially premalignant, state suggest that targeted inhibition of CRIPTO could be beneficial in combination with chemical compounds currently used in clinical practice. Doxorubicin is a single-agent drug that has been the most studied chemotherapy agent for advanced HCC[47]. Despite initial studies showing high response rates, subsequent studies showed only a small survival advantage. It is currently widely used for trans-arterial chemoembolization. The development of combination therapy using molecularly targeting drugs such as sorafenib might be useful for the prevention of early HCC metastasis. Given that sorafenib is the standard of care in advanced stage HCC but provides only a 3-month median survival benefit in advanced stage HCC[46] and no survival benefit in combination with doxorubicin (clinical trial phase III NCT01015833[48]), we explored the possible role of CRIPTO in sorafenib resistance. A low dose of sorafenib did not affect the proliferation of HepG2-CRIPTO cells. These results suggest that CRIPTO causes a differential drug response and refractoriness to sorafenib. This possibility was supported by our finding that HepG2-CRIPTO tumours cultured *ex vivo* possessed areas of proliferating cells following sorafenib treatment.

PDX tissue slices cultured *ex vivo* showed no sensitivity to sorafenib. However, the combination treatment with the N20 peptide, which blocks CRIPTO signalling, showed a significant reduction of proliferation and no effect on apoptosis. This suggests that it might be beneficial to employ a combination of treatments that target either CRIPTO directly or one of its downstream signalling mediators, e.g. ERK and AKT pathways, in order to achieve an inhibition of proliferation in the HCC tumour cells. Similarly, organoids derived from the PDX tumour tissue, treated in the same conditions as the *ex vivo* cultures, showed a reduction in viability when treated with both N20 and sorafenib. This suggests that inhibition of CRIPTO/GRP78 signalling specifically enhances the response to sorafenib. Mechanistically, this effect can be explained by the fact that PI3K/AKT kinase, which is downstream of CRIPTO/GRP78, is also involved in the acquisition of resistance after long exposure to sorafenib[49], while inhibition of AKT may resensitize tumour cells[50]. CRIPTO has been implicated in therapy resistance in lung cancer, with studies showing that high CRIPTO expression correlates with lower sensitivity to treatment with EGFR kinase inhibitors[51,52]. Modulation of CRIPTO expression or downstream (SRC, AKT) signalling reverses the resistance to EGFR inhibitors[52].

The results presented in this study show that CRIPTO signalling increases proliferation and seems to be required for tumour progression, as suggested for both prostate and breast cancer. Our findings suggest that blocking CRIPTO signalling may have therapeutic benefit in combination with existing therapies for HCC.

Acknowledgements

We thank all the members of the Kruithof-de Julio laboratory for critical feedback and specifically we would like to thank Dr Eugenio Zoni for manuscript revision. This work was supported by private funding to M. Kruithof-de Julio and S. Karkampouna.

References

1. Bray F, Jemal A, Grey N, *et al.* Global cancer transitions according to the Human Development Index (2008–2030): a population-based study. *Lancet Oncol* 2012; 13: 790–801.
2. El-Serag HB, Rudolph KL. Hepatocellular carcinoma: epidemiology and molecular carcinogenesis. *Gastroenterology* 2007; 132: 2557–2576.
3. Li D, Kang J, Golas BJ, *et al.* Minimally invasive local therapies for liver cancer. *Cancer Biol Med* 2014; 11: 217–236.
4. European Association for the Study of the Liver, European Organisation for Research and Treatment of Cancer. EASL–EORTC clinical practice guidelines: management of hepatocellular carcinoma. *J Hepatol* 2012; 56: 908–943.
5. Llovet JM, Ricci S, Mazzaferro V, *et al.* Sorafenib in advanced hepatocellular carcinoma. *N Engl J Med* 2008; 359: 378–390.
6. Rahimi RS, Trotter JF. Liver transplantation for hepatocellular carcinoma: outcomes and treatment options for recurrence. *Ann Gastroenterol* 2015; 28: 323–330.
7. Wilhelm SM,Dumas J, Adnane L, *et al.* Regorafenib (BAY73-4506): a neworal multikinase inhibitor of angiogenic, stromal and oncogenic receptor tyrosine kinases with potent preclinical antitumor activity. *Int J Cancer* 2011; 129: 245–255.
8. El-Khoueiry AB, Sangro B, Yau T, *et al.* Nivolumab in patients with advanced hepatocellular carcinoma (CheckMate 040): an open-label, non-comparative, phase 1/2 dose escalation and expansion trial. *Lancet* 2017; 389: 2492–2502.
9. Bruix J, Reig M, Sherman M. Evidence-based diagnosis, staging, and treatment of patients with hepatocellular carcinoma. *Gastroenterology* 2016; 150: 835–853.
10. Behne T, Copur MS. Biomarkers for hepatocellular carcinoma. *Int J Hepatol* 2012; 2012: 7.
11. Gray PC, Harrison CA, Vale W. Cripto forms a complex with activin and type II activin receptors and can block activin signaling. *Proc Natl Acad Sci U S A* 2003; 100: 5193–5198.
12. Gray PC, Shani G, Aung K, *et al.* Cripto binds transforming growth factor β (TGF-β) and inhibits TGF-β signaling. *Mol Cell Biol* 2006; 26: 9268–9278.
13. Gray PC, Vale W. Cripto/GRP78 modulation of the TGF-β pathway in development and oncogenesis. *FEBS Lett* 2012; 586: 1836–1845.
14. Klauzinska M, Castro NP, Rangel MC, *et al.* The multifaceted role of the embryonic gene Cripto-1 in c ancer, stem cells and epithelial–mesenchymal transition. *Semin Cancer Biol* 2014; 29: 51–58.
15. Bianco C, Strizzi L, Rehman A, *et al.* A Nodal- and ALK4-independent signaling pathway activated by Cripto-1 through Glypican-1 and c-Src. *Cancer Res* 2003; 63: 1192–1197.
16. Yeo C-Y, Whitman M. Nodal signals to Smads through Criptodependent and Cripto-independent mechanisms. *Mol Cell* 2001; 7: 949–957.
17. Kruithof-de Julio M, Alvarez MJ, Galli A, *et al.* Regulation of extra-embryonic endoderm stem cell differentiation by Nodal and Cripto signaling. *Development* 2011; 138: 3885–3895.

18. Steelman LS, Chappell WH, Abrams SL, *et al.* Roles of the Raf/MEK/ERK and PI3K/PTEN/Akt/mTOR pathways in controlling growth and sensitivity to therapy – implications for cancer and aging. *Aging (Albany NY)* 2011; 3: 192–222.
19. Kelber JA, Panopoulos AD, Shani G, *et al.* Blockade of Cripto binding to cell surface GRP78 inhibits o ncogenic Cripto signaling via MAPK/PI3K and Smad2/3 pathways. *Oncogene* 2009; 28: 2324–2336.
20. Lee AS. Glucose-regulated proteins in cancer: molecular mechanisms and therapeutic potential. *Nat Rev Cancer* 2014; 14: 263–276.
21. Sun C, Sun L, Jiang K, *et al.* NANOG promotes liver cancer cell invasion by inducing epithelial–mesenchymal transition through NODAL/SMAD3 signaling pathway. *Int J Biochem Cell Biol* 2013; 45: 1099–1108.
22. Spike BT, Kelber JA, Booker E, *et al.* CRIPTO/GRP78 signaling maintains fetal and adult mammary stem cells *ex vivo*. *Stem Cell Reports* 2014; 2: 427–439.
23. Xu C-H, Sheng Z-H, Hu H-D, *et al.* Elevated expression of Cripto-1 correlates with poor prognosis in non-small cell lung cancer. *Tumour Biol* 2014; 35: 8673–8678.
24. Cocciadiferro L, Miceli V, Kang K-S, *et al.* Profiling cancer stem cells in androgen-responsive and refractory human prostate tumor cell lines. *Ann N Y Acad Sci* 2009; 1155: 257–262.
25. Terry S, El-Sayed IY, Destouches D, *et al.* CRIPTO overexpression promotes mesenchymal differentiation in prostate carcinoma cells through parallel regulation of AKT and FGFR activities. *Oncotarget* 2015; 6: 11994–12008.
26. D'Antonio A, Losito S, Pignata S, *et al.* Transforming growth factor alpha, amphiregulin and cripto-1 are frequently expressed in advanced human ovarian carcinomas. *Int J Oncol* 2002; 21: 941–948.
27. Fujii K,YasuiW,Kuniyasu H, *et al.* Expression of CRIPTOin human gall bladder lesions *J Pathol* 1996; 180: 166–168.
28. Giorgio E, Liguoro A, D'Orsi L, *et al.* Cripto haploinsufficiency affects *in vivo* colon tumor development. *Int J Oncol* 2014; 45: 31–40.
29. Strizzi L, Margaryan NV, Gilgur A, *et al.* The significance of a Cripto-1-positive subpopulation of human melanoma cells exhibiting stem cell-like characteristics. *Cell Cycle* 2013; 12: 1450–1456.
30. Wang JH, Wei W, Xu J, *et al.* Elevated expression of Cripto-1 correlates with poor prognosis in hepatocellular carcinoma. *Oncotarget* 2015; 6: 35116–35128.
31. Ji C, Kaplowitz N, Lau MY, *et al.* Liver-specific loss of GRP78 perturbs the global unfolded protein response and exacerbates a spectrum of acute and chronic liver diseases. *Hepatology* 2011; 54: 229–239.
32. Kuo T-C, Chiang P-C, Yu C-C, *et al.* A unique P-glycoprotein interacting agent displays anticancer activity against hepatocellular carcinoma through inhibition of GRP78 and mTOR pathways. *Biochem Pharmacol* 2011; 81: 1136–1144.
33. Chen W-T, Zhu G, Pfaffenbach K, *et al.* GRP78 as a regulator of liver steatosis and cancer progression mediated by loss of the tumor suppressor PTEN. *Oncogene* 2014; 33: 4997–5005.
34. Zoni E, Chen L, Karkampouna S, *et al.* CRIPTO and its signaling partner GRP78 drive the metastatic phenotype in human osteotropic prostate cancer. *Oncogene* 2017; 36: 4739–4749.

35. Karkampouna S, Kloen P, Obdeijn MC, *et al.* Human Dupuytren's *ex vivo* culture for the study of myofibroblasts and extracellular matrix interactions. *J Vis Exp* 2015; (98): 52534.
36. Karkampouna S, Kruithof BP, Kloen P, *et al.* Novel *ex vivo* culture method for the study of Dupuytren's disease: effects of TGFbeta type 1 receptor modulation by antisense oligonucleotides. *Mol Ther Nucleic Acids* 2014; 3: e142.
37. Michalopoulos GK, Bowen WC, Mulè K, *et al.* Histological organization in hepatocyte organoid cultures. *Am J Pathol* 2001; 159: 1877–1887.
38. Huch M, Dorrell C, Boj SF, *et al. In vitro* expansion of single Lgr5+ liver stem cells induced by Wnt-driven regeneration. *Nature* 2013; 494: 247–250.
39. Marumoto T, Tashiro A, Friedmann-Morvinski D, *et al.* Development of a novel mouse glioma model using lentiviral vectors. *Nat Med* 2009; 15: 110–116.
40. Friess H, Yamanaka Y, Buchler M, *et al.* Cripto, a member of the epidermal growth factor family, is over-expressed in human pancreatic cancer and chronic pancreatitis. *Int J Cancer* 1994; 56: 668–674.
41. Wurmbach E, Chen YB, Khitrov G, *et al.* Genome-wide molecular profiles of HCV-induced dysplasia and hepatocellular carcinoma. *Hepatology* 2007; 45: 938–947.
42. Mas VR, Maluf DG, Archer KJ, *et al.* Genes involved in viral carcinogenesis and tumor initiation in hepatitis C virus-induced hepatocellular carcinoma. *Mol Med* 2009; 15: 85–94.
43. Roessler S, Jia HL, Budhu A, *et al.* A unique metastasis gene signature enables prediction of tumor relapse in early-stage hepatocellular carcinoma patients. *Cancer Res* 2010; 70: 10202–10212.
44. Castro NP, Fedorova-Abrams ND, Merchant AS, *et al.* Cripto-1 as a novel therapeutic target for triple negative breast cancer. *Oncotarget* 2015; 6: 11910–11929.
45. de Castro NP, Rangel MC, Nagaoka T, *et al.* Cripto-1: an embryonic gene that promotes tumorigenesis. *Future Oncol* 2010; 6: 1127–1142.
46. Rangel MC, Karasawa H, Castro NP, *et al.* Role of Cripto-1 during epithelial-to-mesenchymal transition in development and cancer. *Am J Pathol* 2012; 180: 2188–2200.
47. Wrzesinski SH, Taddei TH, Strazzabosco M. Systemic therapy in hepatocellular carcinoma. *Clin Liver Dis* 2011; 15: 423–441.
48. Abou-Alfa GK, Johnson P, Knox JJ, *et al.* Doxorubicin plus sorafenib vs doxorubicin alone in patients with advanced hepatocellular carcinoma: a randomized trial. *JAMA* 2010; 304: 2154–2160.
49. Chen KF, Chen HL, Tai WT, *et al.* Activation of phosphatidylinositol 3-kinase/Akt signaling pathway mediates acquired resistance to sorafenib in hepatocellular carcinoma cells. *J Pharmacol Exp Ther* 2011; 337: 155–161.
50. Zhai B, Hu F, Jiang X, *et al.* Inhibition of Akt reverses the acquired resistance to sorafenib by switching protective autophagy to autophagic cell death in hepatocellular carcinoma. *Mol Cancer Ther* 2014; 13: 1589–1598.
51. Zhang H, Zhang B, Gao L, *et al.* Clinical significance of cripto-1 expression in lung adenocarcinoma. *Oncotarget* 2017; 8: 79087–79098.
52. Park K-S, Raffeld M, Moon YW, *et al.* CRIPTO1 expression in EGFR-mutant NSCLC elicits intrinsic EGFR-inhibitor resistance. *J Clin Invest* 2014; 124: 3003–3015.

*53. Zoni E, van der Horst G, van de Merbel AF, *et al.* miR-25 modulates invasiveness and dissemination of human prostate cancer cells via regulation of αv- and α6-integrin expression. *Cancer Res* 2015; 75: 2326–2336.
*54. Karkampouna S, Goumans MJ, Ten Dijke P, *et al.* Inhibition of TGFβ type I receptor activity facilitates liver regeneration upon acute CCl4 intoxication in mice. *Arch Toxicol* 2016; 90: 347–357.
*55. Brunet A, Bonni A, Zigmond MJ, *et al.* Akt promotes cell survival by phosphorylating and inhibiting a Forkhead transcription factor. *Cell* 1999; 96: 857–868.

*Cited only in supplementary material.

Supplementary files

Supplementary materials and methods

RNA isolation, RT-PCR, and quantitative PCR (qPCR)

RNA was isolated using an UltraTurrax homogenizer (T25 basic, IKA, Staufen, Germany) and directly processed according to the TRIpure RNA extraction protocol (Qiagen, Hombrechtikon, Switzerland). Total RNA (0.5 µg) was used for first-strand cDNA synthesis using a RevertAid H Minus first-strand cDNA synthesis kit (Fermentas, LuBio Science, Lucerne, Switzerland). For qPCR, ten-fold diluted cDNA was amplified in a CFX Real Time Detection system (Bio-Rad, Cressier, Switzerland) using SYBR Green Supermix reagent (Bio-Rad). Expression levels were normalized to the transcript of *ACTB*. Primer sequences are indicated in the supplementary material, Table S2.

Migration, measurement of metabolic rate (MTS), and wound-healing assay

Transwell cell migration and aqueous soluble tetrazolium/formazan (Cell Titer Aqueous One solution MTS assay; Promega, Dübendorf, Switzerland) metabolic activity/proliferation assays were performed as described in previous studies[53]. For the wound-healing assay, 500 000 cells per well of a 24-well plate were seeded. After 24 h, the wound was made and the culture medium was refreshed. Subsequently, pictures were taken (4x objective magnification) at 0, 24, 48, and 76 h time points. The size of the wound was measured using ImageJ software and normalized to the time-zero width.

Microscopy and image analysis

Confocal microscopy was performed using a Leica TC-SP5 (Leica Biosystems BV, Amsterdam, The Netherlands) microscope with a 40x 1.4 NA oil-immersion objective. Series of Z stacks were collected and reassembled in ImageJ software (http://rsbweb.nih.gov/ij). Mean fluorescence-positive areas were calculated in ImageJ software using a threshold to select the root boundary and measuring the percentage of positive surface inside the intensity defined by the threshold. For quantification of immunofluorescence signals (LUMC cohort), staining experiments were performed on all samples simultaneously to reduce technical variation and imaged using identical exposure and recording settings. Scoring of the immunohistochemistry of the US Biomax and the Basel TMAs was done by a pathologist, in a blind manner, without any prior information on the clinical and pathological data. The homogeneous staining pattern of the tumour cells was assessed by the pathologist. According to this staining, the tissue received a score of 0 (no staining), 1 (low intensity), 2 (medium intensity), 3 (high intensity) or 4 (strong intensity).

Statistical analysis

Statistical analysis was performed using GraphPad Prism 5.0 software (GraphPad Software, San Diego, CA, USA) and two-way ANOVA tests. Data are presented as mean ± SEM or median and interquartile range (IQR) for non-normally distributed variables. Statistically significant differences are indicated with asterisks (*$p < 0.05$, **$p < 0.01$, ***$p < 0.001$, ****$p < 0.0001$). For qPCR analysis, experiments were repeated at least three times as technical replicates for each sample (different cDNA prearations using the RNA of HepG2 cells or patient tissues) and the average value was calculated. For quantification of the immunofluorescence signal of the stained sections, multiple fields of view were imaged, quantified, and averaged.

Immunofluorescence and immunohistochemistry

Tissues were fixed in 4% paraformaldehyde solution overnight, washed in phosphate buffer saline (PBS), processed for paraffin embedding, and serial paraffin sections of 4 µm were prepared. For antigen retrieval, sections were boiled for 10–30 min in antigen unmasking solution (Vector Labs, Adipogen AG, Liestal, Switzerland) and incubated in 3% H_2O_2 for endogenous peroxidase inactivation. Sections were blocked with 1% bovine serum albumin in PBS + Tween 20 (0.1%, v/v) and subsequently incubated with primary antibodies diluted in the blocking solution, overnight at 4°C. The primary antibodies and dilutions used were as follows: anti-CRIPTO, 1:2000 and anti-GRP78, 1:1000 (kindly provided by Dr Peter Gray), anti-αSMA, 1:500 (A2547, clone 1A4; Sigma, Buchs, Switzerland), anti-PCNA, 1:500 (P8825, clone PC 10; Sigma), anti-cleaved CASPASE 3, 1:500 (9661; Cell Signaling, BioConcept Allschwil, Switzerland), and anti-HNF4a, 1:100 (sc-6556, clone C19; Santa Cruz, LabForce, Muttenz, Switzerland). The following day, sections were incubated with secondary antibodies labelled with Alexa Fluor 488, 555, or 647 (Invitrogen/Molecular Probes, Zurich, Switzerland; 1:250 in PBS + 0.1% Tween 20). Detection of CRIPTO and GRP78 was enhanced using tyramide amplification (Invitrogen/Molecular Probes) as described previously[54]. Sections were counterstained with TO-PRO-3 (Invitrogen/Molecular Probes) or DAPI solution (Sigma) for visualization of nuclei, and mounted using Prolong G mounting medium (Invitrogen/Molecular Probes). For CRIPTO immunohistochemistry, the TMA samples were deparaffinized and antigen retrieval was performed by boiling (microwave, 240 W) in 10 mM Tris–HCl containing 1 mM EDTA (pH 9.0) buffer for 30 min. Endogenous peroxidases were blocked using 3% H_2O_2–15 mM NaN_3 for 5 min at room temperature. Sections were blocked with swine serum and incubated with primary anti-CRIPTO antibody [diluted 1:1000 in 0.5% swine serum in antibody diluent buffer (DAKO)]. Secondary anti-rabbit HRP was used (Envision system) for 30 min at room temperature. Signal was developed using AEC substrate (Sigma #A6926, 20 mg) diluted in 10% DMN, 10% imidazole buffer, and 0.02% H_2O_2.

Reporter assays

To assess AKT pathway activation, the FOXO-luc reporter assay was used. The FOXO-luc construct (Addgene, #1789) contains the promoter response element of the Forkhead box

transcription factor gene *FOXO3* (FKHRL), which controls the expression of luciferase [55]. When AKT is active, it phosphorylates FOXO3 and blocks downstream FOXO transcription activation. Thus, FOXO-luc activation occurs when AKT is inactive. HepG2-CRIPTO cells were transfected with 500 ng of FOXO plasmid and 5 ng of *Renilla* plasmid in 24-well plates using DharmaFect I reagent (ratio to DNA 4:1) in Optimem medium. After 16 h, cells were treated with vehicle (10% DMSO) plus IgG (2 µg/ml, R&D goat IgG), 20% FCS, sorafenib (1 µM), GRP78 antibody (2 µg/ml, A-10 Abcam), and N20 blocking peptide (2 µg/ml, Santa Cruz). Cells were lysed after 6 h of treatment with 100 µl of passive cells lysis (Promega). Lysates (10 µl) were transferred into opaque 96-well plates in triplicate per sample. Luciferase buffer (LAR-II, 25 µl) was added to the lysates and luciferase activity was measured after 10 min. An equal amount of STOP&Glo reagent was added and *Renilla* firefly activity was measured after 10 min. Values were normalized to cell lysis buffer as a control and to the *Renilla* counts. Mean fold-change values were calculated over the DMSO/IgG control.

Western immunoblotting

Cells were lysed in cold RIPA lysis buffer [10 mM Tris (pH 8.0), 140 mM NaCl, 1% Triton-X 100, 0.1% $C_{24}H_{39}NaO_4$, 1 mM EDTA (pH 8.0), 0.1% SDS, 1 mM EGTA plus complete protease inhibitors; Roche] using a cell scraper. Lysates were passed through a 26-gauge needle. Following a centrifugation step (15 min, 4000 rpm, 4°C) to remove debris, the protein extract was collected (supernatant). Protein content was quantified using a DC protein assay (Bio-Rad) using serial dilutions of BSA in tissue lysis buffer. A total of 30 µg was diluted in 4´ Laemmli buffer, separated by SDS-PAGE, and transferred to PVDF membranes. The following primary antibodies were used in 5% bovine serum albumin diluted in TBS + 0.1% Tween 20: anti-PCNA, 1:5000 (P8825, clone PC 10; Sigma) anti-CRIPTO, 1:1000 and anti-GRP78, 1:1000 (kindly provided by Dr Peter Gray), tubulin, 1:3000 (T8578, clone 2G10; Sigma), and anti-pAKT (S473), 1:1000 (9271S, Cell Signaling). Appropriate secondary HRP antibodies (Promega) were used and detected by chemiluminescence (Bio-Rad).

Supplementary Table S1. Organoid media composition

	Final concentration
Advanced DMEM/F12 (supplemented with PenStrep, GlutaMAX, Hepes, and primocin)	
FCS	5%
Y-27632	10 μM
A83-01	500 nM
SB202190	10 μM
R-spondin	500 ng/ml
Noggin	100 ng/ml
B27	1´
N-acetyl-cysteine	1.25 mM
Nicotinamide	10 mM
EGF	50 ng/ml
FGF10	10 ng/ml
Wnt3A	100 ng/ml
HGF	50 ng/ml

Supplementary Table S2. Primer sequences used in this study

Primer	Forward	Reverse
ALDH1A1 (human)	TGGCTTATCAGCAGGAGTGT	GCAATTCACCCACACTGTTC
ALK4 (human)	GCTCGAAGATGCAATTCTGG	TTGGCATACCAACACTCTCG
αv INTEGRIN (human)	GCTGGACTGTGGAGAAGAC	AAGTGAGGTTCAGGGCATTC
β-actin (human)	AATGTCGCGGAGGACTTTGATTGC	GGATGGCAAGGGACTTCCTGTAAA
β-actin (mouse)	GGGGTGTTGAAGGTCTCAAA	AGAAAATCTGGCACCCC
BMI-1 (human)	TCATCCTTCTGCTGATGCTG	CCGATCCAATCTGTTCTGGT
β3 INTEGRIN (human)	GTCTGCCACAGCAGTGACTT	CTTGTAGCGGACACAGGAGA
CD24 (human)	TACCCACGCAGATTTATT	AGAGTGAGACCACGAAGA
CD44 (human)	TGGCACCCGCTATGTCCAG	GTAGCAGGGATTCTGTCTG
Cripto (mouse)	CGCCAGCTAGCATAAAAGTG	CCCAAGAAGTGTTCCCTGTG
CRIPTO (human)	CACGATGTGCGCAAAGAGAA	TGACCGTGCCAGCATTTACA
E-CADHERIN (human)	TTGACGCCGAGAGCTACAC	GACCGGTGCAATCTTCAAA
EPCAM (mouse)	AGGGGCGATCCAGAACAACG	ATGGTCGTAGGGGCTTTCTC
GLI-1 (human)	CTGGTGGCTTTCATCAACTCTC	GGTACACAGGGCTGGACTC
GRP78 (human)	GAACGTCTGATTGGCGATGC	TCAACCACCTTGAACGGCAA
LEFTY (human)	CGAGTGGCTGCGCGTCCGCGA	CGAGGCACAGCTGCACTTCTGCACC
N-CADHERIN (human)	CAGACCGACCCAAACAGCAAC	GCAGCAACAGTAAGGACAAACATC
NANOG (human)	AATACCTCAGCCTCCAGCAGATG	TGCGTCACACCATTGCTATTCTTC
NODAL (human)	CTTCTCCTTCCTGAGCCAACAAGAGG	GGTGACCTGGGACAAAGTGACAGTG
OCT4 (human)	GAGAACCGAGTGAGAGGCAACC	CATAGTCGCTGCTTGATCGCTTG
SNAIL-2 (human)	TGTGTGGACTACCGCTGC	TCCGGAAAGAGGAGAGAGG
SOX2 (human)	CAGGAGTTGTCAAGGCAGAGA	CGCCGCCGATGATTGTTATTA
TWIST (human)	GCCGGAGACCTAGATGTCATT	TTTTAAAAGTGCGCCCCACG
VIMENTIN (human)	CCAAACTTTTCCTCCCTGAACC	CGTGATGCTGAGAAGTTTCGTTGA
ZEB-1(human)	CCATATTGAGCTGTTGCCGC	GCCCTTCCTTTCCTGTGTCA
ZEB-2 (human)	GACCTGGCAGTGAAGGAAAA	GGCACTTGCAGAAACACAGA

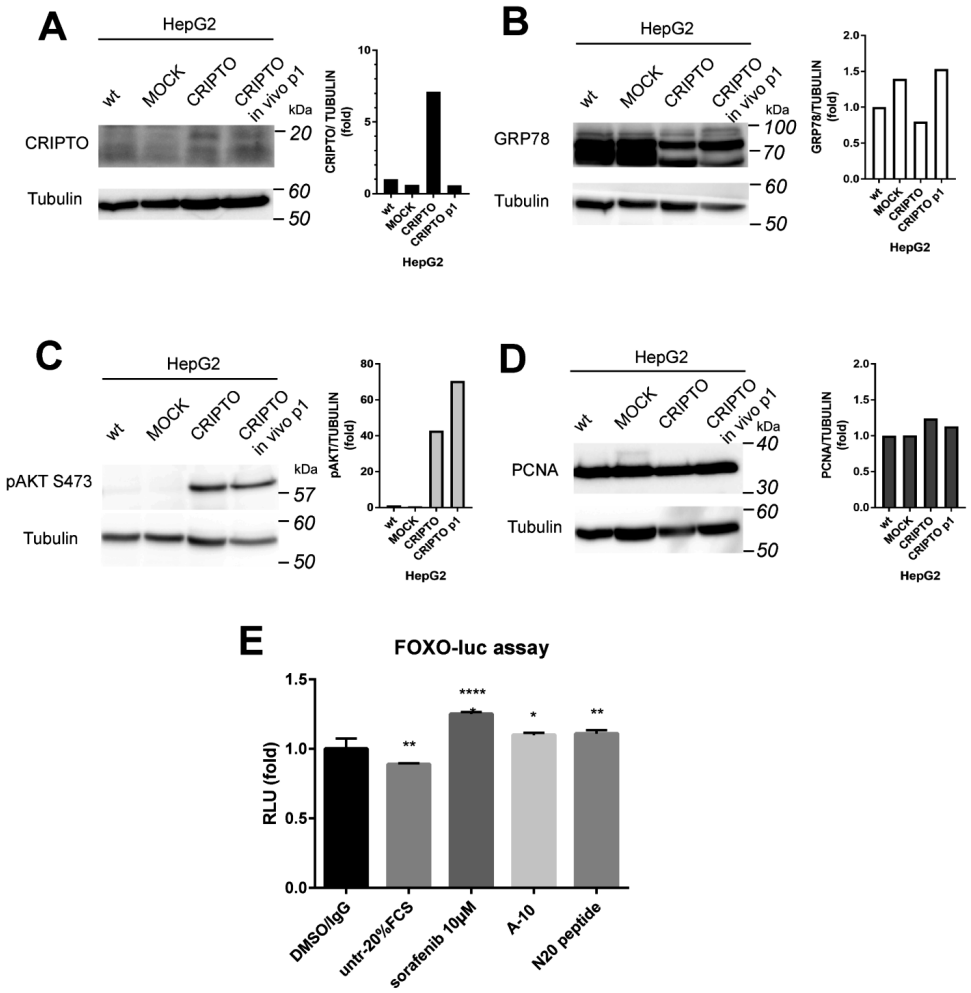

Supplemental Figure 1. *In vitro* characterisation of CRIPTO downstream pathway activation. (A–D) Western blotting and corresponding quantifications for CRIPTO (A), GRP78 (B), phosphorylated AKT (pAKT) (C), and PCNA (D) in HepG2, HepG2-MOCK, HepG2-CRIPTO cells, and HepG2-CRIPTO cells after *in vivo* passaging. Tubulin was used to assess equal protein loading. (E) Reporter FOXO assay for AKT pathway activation determination in the HepG2-CRIPTO cells.

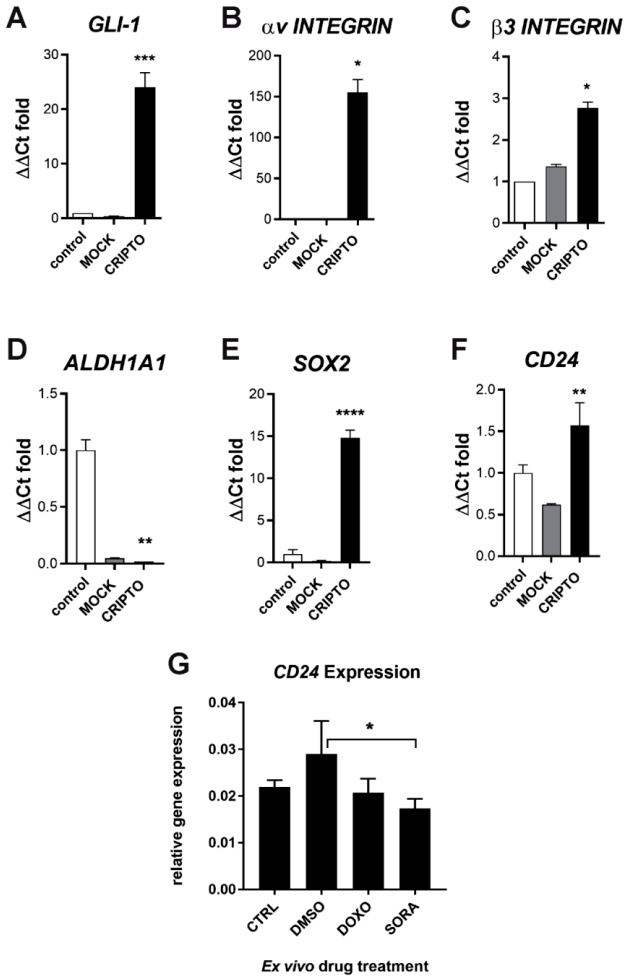

Supplemental Figure 2. Expression of stem cell markers in CRIPTO-overexpressing cells. (A–F) mRNA expression of stem cell markers in HepG2 (control), HepG2-MOCK, and HepG2-CRIPTO cell lines: (A) *GLI1*, (B) αv INTEGRIN (*ITGAV*), (C) β3 INTEGRIN (*ITGB3*), (D) *ALDH1A1*, (E) *SOX2*, (F) *CD24*. (G) mRNA levels of *CD24* after e*x vivo* culture of HepG2-CRIPTO tumour slices after treatment with vehicle (DMSO), doxorubicin (DOXO) or sorafenib (SORA). CTRL: no treatment control. Error bars indicate ± SD. **p* < 0.05.

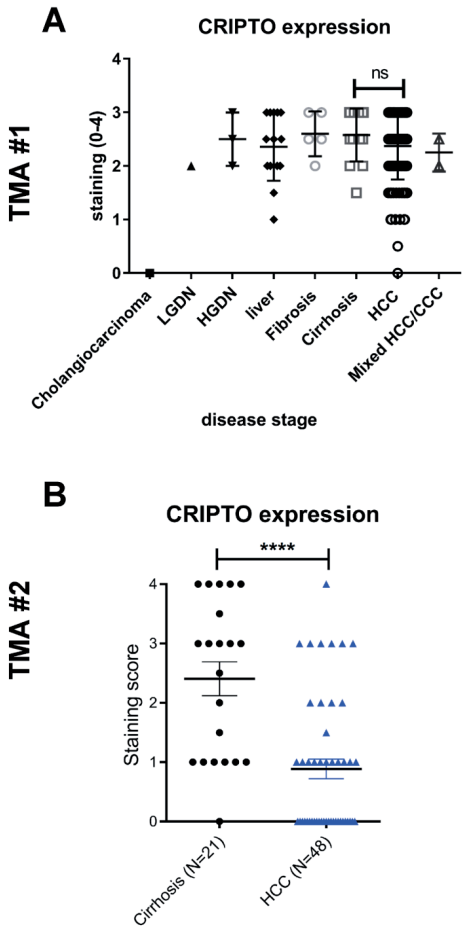

Supplemental Figure 3. CRIPTO staining in HCC versus non-HCC cases of two TMAs. CRIPTO staining scoring after pathologist's evaluation of (A) TMA (Basel) with HCC and non-HCC cases (tumour-adjacent tissues from fibrosis, cirrhosis, cholangiocarcinoma, and low-grade and high-grade dysplastic nodule cases) and (B) TMA (US Biomax) containing cirrhosis and HCC cases. Error bars indicate ± SEM. ****$p < 0.0001$.